Low magnetic Prandtl number dynamos with helical forcing

Pablo D. Mininni[1] and David C. Montgomery[2]
[1]*National Center for Atmospheric Research, P.O. Box 3000, Boulder, Colorado 80307, USA*
[2]*Department of Physics and Astronomy, Dartmouth College, Hanover, New Hampshire 03755, USA*
(Received 5 May 2005; published 18 November 2005)

We present direct numerical simulations of dynamo action in a forced Roberts flow. The behavior of the dynamo is followed as the mechanical Reynolds number is increased, starting from the laminar case until a turbulent regime is reached. The critical magnetic Reynolds for dynamo action is found, and in the turbulent flow it is observed to be nearly independent on the magnetic Prandtl number in the range from ~0.3 to ~0.1. Also the dependence of this threshold with the amount of mechanical helicity in the flow is studied. For the different regimes found, the configuration of the magnetic and velocity fields in the saturated steady state are discussed.

DOI: 10.1103/PhysRevE.72.056320 PACS number(s): 47.65.+a, 47.27.Gs, 95.30.Qd

I. INTRODUCTION

In a previous publication [1], a driven turbulent magnetohydrodynamic (MHD) dynamo was studied numerically, within the framework of rectangular periodic boundary conditions. The emphasis was on the dynamo's behavior as the magnetic Prandtl number P_M (ratio of kinematic viscosity to magnetic diffusivity) was lowered. As P_M is lowered at fixed viscosity, the magnetofluid becomes more resistive than it is viscous, and it is intuitively apparent that magnetic fields will be harder to excite by mechanical motions. The principal result displayed in Ref. [1] was a curve of critical magnetic Reynolds number, R_M^c, as a function of P_M^{-1}, at fixed kinetic energy. The (turbulent) kinetic energy was the result of an external mechanical forcing of the Taylor-Green type (hereafter, "TG"), a geometry well known to be efficient at the rapid generation of small scales in the fluid flow [2]. Reference [1] contains a lengthy bibliography of its antecedents, not all of which will be listed again here.

The TG geometry injects no net mechanical helicity into the flow. In the long history of the dynamo problem, mechanical helicity has been seen often to be an important ingredient for dynamo action, and it is the intent of this present paper to consider a helically forced dynamo in the same spirit as in Ref. [1], to see what changes occur relative to the TG flow, further properties of which were displayed in a subsequent astrophysical paper [3].

A natural candidate for a highly helical velocity field is what has come to be called the "Roberts flow" [4,5]. This flow shares some similarities with the dynamo experiments of Riga and Karlsruhe [6,7]. In a pioneering paper [8], Feudel *et al.* characterized mathematically various magnetic-field-generating instabilities that a forced Roberts flow can experience. The present paper expands these investigations, while discussing numerical simulation results for magnetic excitations in the mechanically turbulent regime, with an emphasis on the nonlinearly saturated magnetic field configuration. As in Ref. [8], we will force the system at nearly the largest scale available in the periodic domain. As a result, magnetic fields will be only amplified at scales smaller than the energy containing scale of the flow. The behavior of the large-scale dynamo (i.e., when magnetic perturbations are amplified at scales larger than the energy containing eddies) as P_M is varied will be studied in a future work.

Section II provides the dynamical equations and definitions and describes the methodology to be used in the numerical study. Section III presents results and compares some of them with the corresponding TG results. Section IV summarizes and discusses what has been presented, and points in directions that we believe the results suggest. An Appendix describes the differences between critical magnetic Reynolds numbers calculated on the basis of instantaneous flows and on the basis of the time averages of these flows; these can be considerable.

II. MATHEMATICAL FRAMEWORK AND METHODOLOGY

In a familiar set of dimensionless ("Alfvénic") units the equations of magnetohydrodynamics to be solved are

$$\frac{\partial \mathbf{v}}{\partial t} + \mathbf{v}\cdot\nabla\mathbf{v} = -\nabla\mathcal{P} + \mathbf{j}\times\mathbf{B} + \nu\nabla^2\mathbf{v} + \mathbf{f}, \tag{1}$$

$$\frac{\partial \mathbf{B}}{\partial t} + \mathbf{v}\cdot\nabla\mathbf{B} = \mathbf{B}\cdot\nabla\mathbf{v} + \eta\nabla^2\mathbf{B}, \tag{2}$$

with $\nabla\cdot\mathbf{v}=0$, $\nabla\cdot\mathbf{B}=0$. $\mathbf{v}$ is the velocity field, regarded as incompressible (low Mach number). $\mathbf{B}$ is the magnetic field, related to the electric current density $\mathbf{j}$ by $\nabla\times\mathbf{B}=\mathbf{j}$. $\mathcal{P}$ is the normalized pressure-to-density ratio, obtained by solving the Poisson equation for it that results from taking the divergence of Eq. (1) and using the incompressibility condition $\nabla\cdot\mathbf{v}=0$. In these units, the viscosity ν and magnetic diffusivity η can be regarded as the reciprocals of mechanical Reynolds numbers and magnetic Reynolds numbers, respectively, where these dimensionless numbers in laboratory units are $R_V=LU/\nu_{\rm lab}$, $R_M=LU/\eta_{\rm lab}$. Here U is a typical turbulent flow speed (the rms velocity in the following sections), L is a length scale associated with its spatial variation (the integral length scale of the flow), and $\nu_{\rm lab}$, $\eta_{\rm lab}$ are kinematic viscosity and magnetic diffusivity, respectively, ex-

pressed in dimensional units. In the next sections, all the figures and quantities discussed will follow this convention and will be given in Alfvénic dimensionless units. The external forcing function **f** is to be chosen to supply kinetic energy and kinetic helicity and to maintain the velocity field **v**.

For **f**, we choose in this case the Roberts flow [4,8],

$$\mathbf{f} = -\nu\nabla^2\mathbf{v}_R = 2\nu\mathbf{v}_R, \tag{3}$$

where

$$\mathbf{v}_R = (g\sin x\cos y, -g\cos x\sin y, 2f\sin x\sin y). \tag{4}$$

The coefficients f and g are arbitrary and their ratio determines the extent to which the flow excited will be helical. The ratio $f=g/\sqrt{2}$ is maximally helical for a given kinetic energy, and the case $f/g\to 0$ is a (two-dimensional) nonhelical excitation. We have concentrated primarily upon the cases $f=g$ (following Feudel *et al.* [8]) and $f=g/\sqrt{2}$. No dynamo can be expected unless $|f/g|>0$.

We impose rectangular periodic boundary conditions throughout, using a three-dimensional periodic box of edge 2π, so that the fundamental wave number has magnitude 1. All fields are expanded as Fourier series, such as

$$\mathbf{v} = \mathbf{v}(\mathbf{x},t) = \sum_{\mathbf{k}} \mathbf{v}(\mathbf{k},t)\exp(i\mathbf{k}\cdot\mathbf{x}) \tag{5}$$

with $\mathbf{k}\cdot\mathbf{v}(\mathbf{k},t)=0$. The Fourier series are truncated at a maximum wave number $k_{\max}$ that is adequate to resolve the smallest scales in the spectra. The method used is the by-now familiar Orszag-Patterson pseudospectral method [9–11]. The details of the parallel implementations of the fast Fourier transform can be found in Ref. [12].

The forcing function (4) injects mechanical energy at a wave number $|\mathbf{k}|=\sqrt{2}$, which leaves very little room in the spectrum for any back-transfer of helicity ($|\mathbf{k}|=1$ is the only possibility). The phenomena observed will therefore be well separated from those where an "inverse cascade" of magnetic helicity is expected to be involved. Rather, a question that can be answered (in the affirmative, it will turn out) is whether the presence of mechanical helicity makes it easier to excite magnetic fields through turbulent dynamo action.

Equations (3) and (4) define a steady state solution of Eqs. (1) and (2), with $\mathbf{B}=\mathbf{0}$. It is to be expected that for large enough ν and η, this solution will be stable. As the transport coefficients are decreased, it will be the case that the flow of Eq. (4) can become unstable, either purely mechanically as an unstable Navier-Stokes flow, or magnetically as a dynamo, or as some combination of these. Thus rather complex scenarios can be imagined as either of the Reynolds numbers is raised.

In the following, the emphasis will be upon discovering thresholds in R_M at which dynamo behavior will set in as R_V is raised, then further computing the nonlinear regime and saturation of the magnetic excitations once it does. The "growth rate" σ can be defined as $\sigma = d\ln(E_M)/dt$, where $E_M=\Sigma_{\mathbf{k}}|\mathbf{B}(\mathbf{k},t)|^2/2$ is the total magnetic energy. The appearance of a positive σ for initially very small E_M is taken to define the critical magnetic Reynolds number R_M^c for the onset of dynamo action. σ is typically expressed in units of the reciprocal of the large-scale eddy turnover time L/U where U is the rms velocity ($U=\langle u^2\rangle^{1/2}$, and the brackets denote spatial average), and L is the integral length scale,

$$L = 2\pi\sum_{\mathbf{k}} k^{-1}|\mathbf{u}(\mathbf{k},t)|^2 \Big/ \sum_{\mathbf{k}} |\mathbf{u}(\mathbf{k},t)|^2. \tag{6}$$

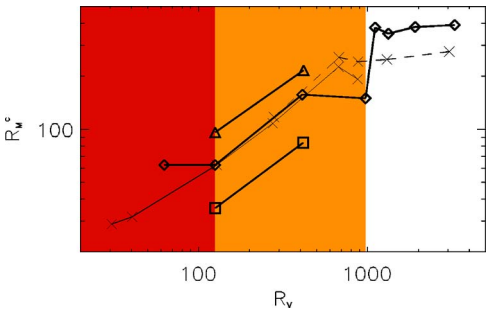

FIG. 1. (Color online) Critical magnetic Reynolds R_M^c as a function of R_V for different Roberts flows (thick lines), $f=g$ ($\diamond$), $f=g/\sqrt{2}$ ($\square$), $f=g/0.77$ ($\triangle$). The dark (red) area corresponds to the region where the Roberts flow is hydrodynamically stable. For a comparison with Ref. [8], our Reynolds numbers should be divided by 2π. The light (orange) area corresponds to the region of hydrodynamic oscillations, while the white area corresponds to the turbulent regime. The thin lines connected with crosses are shown as a reference and correspond to the threshold for dynamo instability in Taylor-Green flow [1], DNS (solid line) and α model (dashed line).

In the next section, we describe the results of the computations for both the "kinematic dynamo" regime [where $\mathbf{j}\times\mathbf{B}$ is negligible in Eq. (1)], and for full MHD where the Lorentz force modifies the flow.

III. DYNAMO REGIMES FOR THE ROBERTS FLOW

We introduce the results for the Roberts flow through a plot of the threshold values of critical magnetic Reynolds number R_M^c vs mechanical Reynolds number R_V (Fig. 1). All Reynolds numbers have been computed using the integral scale for the velocity field [Eq. (6)], averaged over the duration of the steady state in the hydrodynamic simulation. For each set of simulations at a given R_V, an overall normalization factor has been multiplied by Eq. (3) to make the rms velocity U turn out to have a time averaged value of order 1 in the hydrodynamic turbulent steady state. This election was made only for numerical convenience; note that no scheme was used to vary the amplitude of the external force in time as in Ref. [3], and the normalization factor in front of Eq. (3) was held constant (and independent of time) for all hydrodynamic and MHD runs at the same value of R_V.

Figure 1 contains considerable information. There are basically three qualitative behaviors exhibited for different R_V, indicated by the (colored) background shading. For $R_V \lesssim 100$, the laminar Roberts flow is hydrodynamically steady state and laminar, but dynamo action is still possible for large enough R_M. For $100\lesssim R_V\lesssim 1000$, Roberts flow treated purely hydrodynamically is temporally periodic but not turbulent. For $R_V\gtrsim 1000$, the Roberts flow develops a full turbulent spectrum hydrodynamically. In all three regimes, dy-

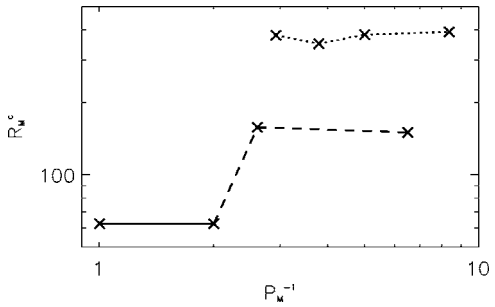

FIG. 2. Critical magnetic Reynolds R_M^c as a function of P_M^{-1} for the Roberts flow with $f=g$ (thick lines). The solid line corresponds to the laminar regime ($R_V \lesssim 100$), the dashed line to the periodic flow ($100 \lesssim R_V \lesssim 1000$), and the dotted line to the turbulent regime ($R_V \gtrsim 1000$). The double-valuedness results from the effects of two different values of R_V.

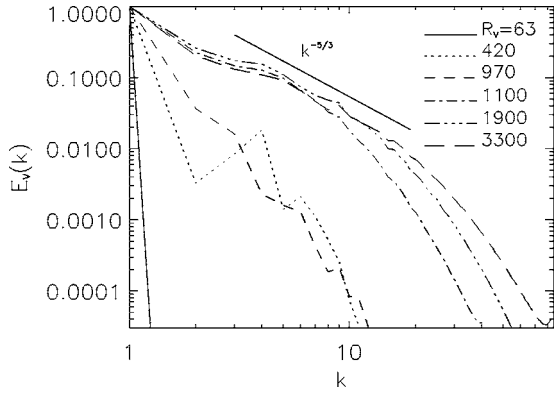

FIG. 3. Kinetic energy spectra as a function of R_V. The Kolmogorov's spectrum is shown as a reference.

namo action is exhibited, but is different in the three regimes. The laminar regime was extensively studied in Ref. [8]. Our definitions for the Reynolds numbers are different, but the results displayed in Figs. 1 and 2 are consistent with previous results in the range $P_M=[0.5,1]$ if our Reynolds numbers are divided by 2π (corresponding approximately to the integral scale of the laminar flow).

The threshold curve connecting diamonds ($\diamond$) is for the Roberts flow with $f=g$ (helical, but not maximally so). The segment connecting squares ($\square$) is for $f=g/\sqrt{2}$ (maximal helicity). The segment connected by triangles ($\triangle$) is for $f=g/0.77$, a less helical flow than $f=g$. The threshold curve connecting crosses ($\times$) is the threshold curve for the Taylor-Green (TG) flow from Ref. [1]. All of these are direct numerical simulation (DNS) results. (We regard the fact that the Taylor-Green curve and the Roberts flow curve with $f=g$ have a common region above $R_V \sim 100$ to be coincidental.) The curve connecting crosses ($\times$) with a dashed line is the result from Ref. [1] for the "α model," or Lagrangian averaged model, of MHD.

Noteworthy in Fig. 1 is the qualitative similarity of the behavior of the threshold curve between the Roberts flow and the TG results from Ref. [1], a sharp rise in R_M^c with the increase in the degree of turbulence in the velocity field, followed by a plateau in which further increases in R_V show little effect upon R_M^c.

Figure 2 shows the threshold curve for the Roberts flow with $f=g$ as a function of the inverse of the magnetic Prandtl number, P_M^{-1}. This curve shares some similarities with the TG flow, but also important differences. As in Ref. [1], between the laminar and turbulent regimes a sharp increase in R_M^c is observed. Also, in the turbulent flow R_M^c seems to be independent of the value of the magnetic Prandtl number. But while the TG force is not a solution of the Euler equations and was designed to generate smaller and smaller scale fluctuations as the Reynolds number R_V is increased, the Roberts flow goes through several instabilities as R_V is varied. As a result, the threshold for dynamo action in the R_M vs P_M^{-1} plane is double valued. For a given value of P_M^{-1} two values of R_M^c exist according to the hydrodynamic state of the hydrodynamic system, (e.g., laminar, periodic, or turbulent flow).

The double valuedness apparent in Fig. 2 is due to the fact that there are more relevant fluid variables involved than a two-dimensional plot permits us to display. The Roberts flow exhibits pure hydrodynamic instabilities that occur as the mechanical Reynolds number R_V is raised in a given substance, instabilities not directly involving either P_M or R_M. One can imagine a third axis perpendicular to the plane shown corresponding to R_V. Proceeding outward along this direction would correspond to an experimentalist's forcing the fluid more strongly, leaving the other features of his experiment the same. As R_V increases in this perpendicular direction, one passes from a laminar to a periodic to a turbulent regime for the fluid. The two horizontal lines in Fig. 2 correspond to the computed values of critical magnetic Reynolds number for the onset of dynamo action in the periodic regime (bottom dashed curve) and in the turbulent regime (top dotted curve). It is possible to pass outside the dynamo-unstable periodic regime before crossing into the dynamo-unstable turbulent regime. The crosses do not necessarily correspond to the same values of RV. These "windows" where no dynamo action can take place are reminiscent of the behavior of "ABC" dynamos at low RM (e.g., Ref. [13]). Note, however, that for the Roberts flow, this double-valued "window" behavior occurs in the R_M-P_M plane, not in the R_M-R_V plane, as observed in Ref. [13].

Figure 3 is a plot of the kinetic energy spectra for the values of R_V shown in Fig. 1, for $f=g$, normalized so that $E_V(k=1)$ is unity for all cases. This is done to display the gradual widening of the spectrum as R_V increases. Figure 4 shows corresponding magnetic spectra, normalized somewhat differently, the energy contained in the interval $1 \leqslant k \leqslant 5$ is the same in all cases. This is done to emphasize the fact that the peak in the magnetic energy spectrum migrates to higher values as R_V increases, the excited magnetic field develops more and more small-scale features. This may be related to the fact that because the forcing occurs at such low wave numbers, inverse magnetic helicity cascades are effectively ruled out.

Figure 5 shows how the thresholds ($\sigma=0$) for the R_M^c curves were calculated. For small initial E_M, broadly distributed over k, η was gradually decreased in steps to raise R_M in the same kinetic setting until a value of $\sigma \approx 0$ was identified. A linear fit between the two points with σ closest to 0 pro-

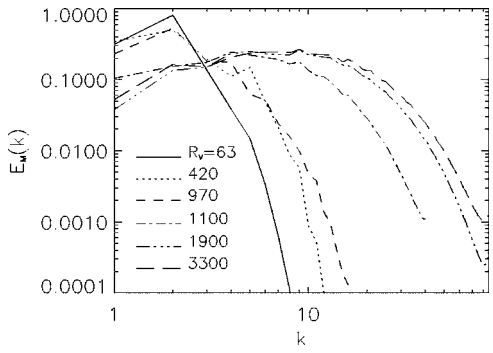

FIG. 4. Magnetic energy spectra during the kinematic regime, for different values of R_V. The values of R_M for each curve correspond to the smallest value for which dynamo action was observed (see Fig. 5).

vides a single point on such curves as those in Fig. 1. Figure 5 also gives bounds for the uncertainties in the determination of the threshold R_M^c (see, e.g., Ref. [1]), errors in Fig. 1 are defined as the distance between the value of R_M^c and the value of R_M in the simulation with σ closest to 0. In general, the errors in R_M^c are of the order of 2% in the laminar runs [dark (red) shaded area in Fig. 1], 8% in the oscillatory runs [light (orange) shaded area in Fig. 1], and 15% in the turbulent runs (white area in Fig. 1). The increase in the error is the result of the increasing difficulty to identify small values of σ in the turbulent regime because of the fluctuations in the energy as a function of time.

Each simulation at a fixed value of ν and η (or fixed R_V and R_M) was extended for at least 100 large-scale turnover times to rule out turbulent fluctuations and obtain a good fit to the exponential growth. All the simulations were well resolved and satisfied the condition $k_\nu/k_{\max}<1$, where $k_\nu=(\epsilon/\nu^3)^{1/4}$ is the Kolmogorov dissipation wave number, ϵ is the energy injection rate, $k_{\max}=N/3$ is the largest resolved wave number, and N is the linear resolution of the simulation. When this condition was not satisfied, the resolution N was increased, from $N=64$ until reaching the maximum spatial resolution in this work of 256 grid points in each direction, and a maximum mechanical Reynolds of $R_V=3300$.

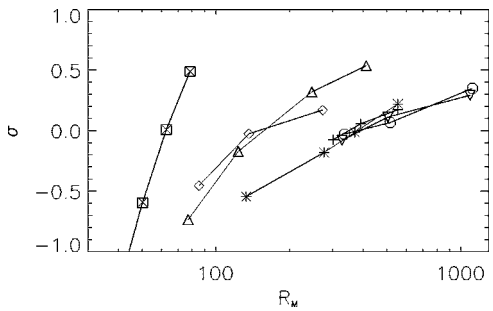

FIG. 5. Growth rates as a function of R_M. Each line corresponds to several simulations at constant R_V (fixed ν), and each point in the line indicates the exponential growth (or decay) rate at a fixed value of R_M. The point where each curve crosses $\sigma=0$ gives the threshold R_M^c for dynamo instability. $R_V=63$ (□), $R_V=130$ (×), $R_V=420$ (△), $R_V=970$ (◇), $R_V=1100$ (*), $R_V=1300$ (+), $R_V=1900$ (○), and $R_V=3300$ (▽).

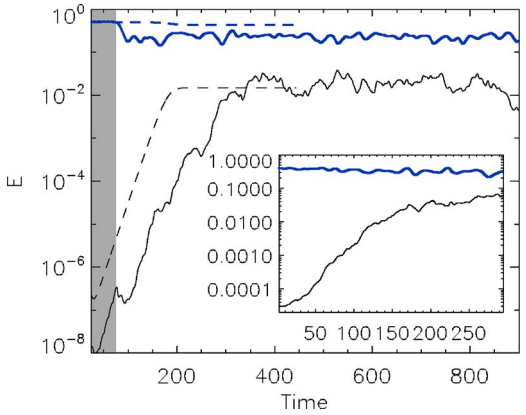

FIG. 6. (Color online) Time history of the total kinetic [thick (blue) lines] and magnetic energy (thin lines) in dynamo simulations. The dashed lines correspond to $R_V=63$ and $R_M=79$ (laminar flow), while the solid lines are for $R_V=R_M=420$. The shaded region indicates the period of time when the flow is oscillating in this simulation. The inset shows the time history for a turbulent run with $R_V=3300$ and $R_M=1100$.

Figure 6 illustrates an interesting behavior that occurs when there is a transition from the laminar to the periodic regime of the Roberts flow ($f=g$). Figure 6 shows the evolution of total kinetic energies E_V and magnetic energies E_M for $R_V=63$ and $R_V=420$. The flat part of the kinetic [thick (blue)] curve for $R_V=420$ is characterized by small periodic oscillations too small to see on the logarithmic plot (they will be shown in Fig. 7). Meanwhile, the E_M curve of magnetic energy is growing, somewhat irregularly. Rather suddenly, at about $t=70$, E_V drops by more than a factor of 2 (see Fig. 7), and by $t\approx 300$ the magnetic energy has saturated at a level of about 1 percent of the initial kinetic energy. Both fields oscillate irregularly after that, and are weakly turbulent. It is unclear how such a small magnetic excitation succeeds at shutting down such a large fraction of the flow. As will be shown later, this large drop is associated with the instability of the large scale flow. The inset shows the full time history of E_V and E_M, for $R_V=3300$ and $R_M=1100$ when the turbulence is fully developed. The dashed line illustrates, for comparison, how simply the magnetic energy exponentiates and saturates in the laminar steady-state regime ($R_V=63$). Figure 7 shows in detail the suppression of the flow, manifested as a drop in the total energy, at $t\approx 70$.

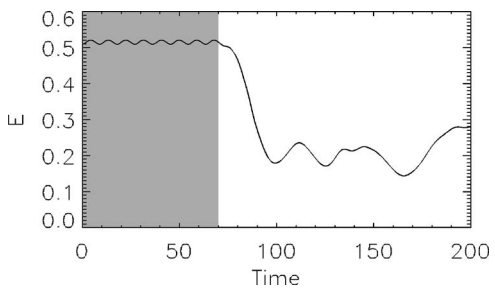

FIG. 7. Time history of the total energy in the dynamo simulation with $R_V=R_M=420$. The shaded area is a blow up of the shaded region in Fig. 6 and corresponds to the hydrodynamic oscillations.

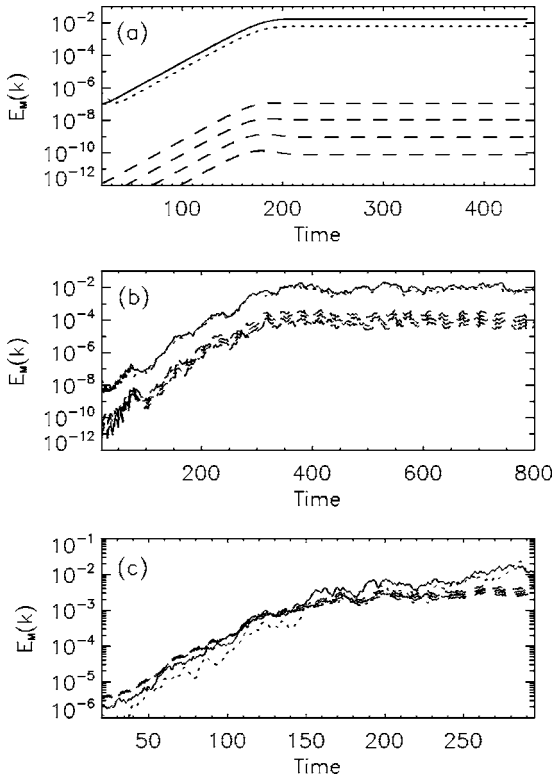

FIG. 8. Evolution of the magnetic energy in different shells in Fourier space: (a) $R_V=63$ and $R_M=78$ (laminar flow), (b) $R_V=R_M=420$ (periodic case), (c) $R_V=3300$ and $R_M=1100$ (turbulent regime). The dotted line corresponds to $k=1$, solid line to $k=2$, and the dashed lines to $k=9,10,11,12$.

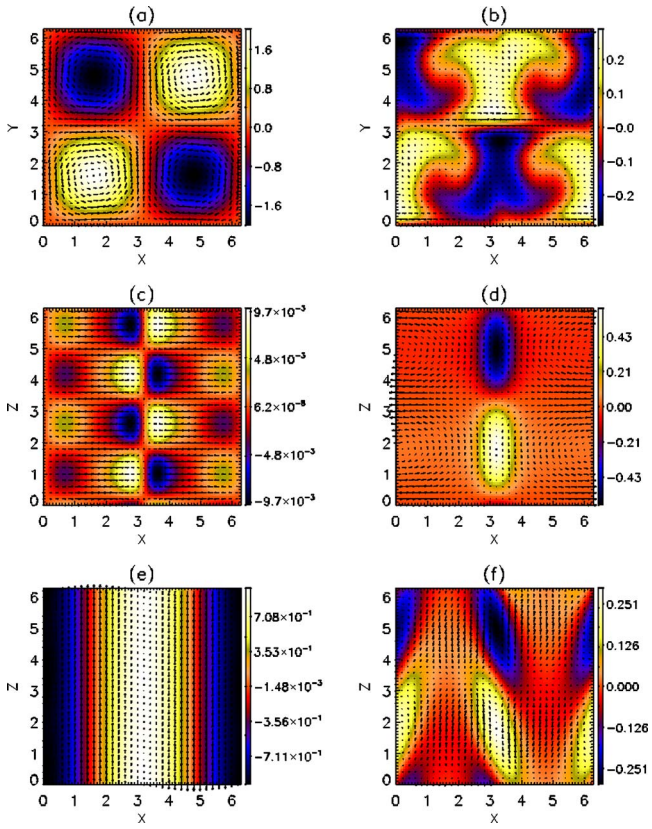

FIG. 9. (Color online) Plots of the kinetic and magnetic fields for the saturated regime of the run with $R_V=63$ and $R_M=78$, (a) cut at $z=0$, vz in color and vx, vy indicated by arrows, (b) same as in (a) for the magnetic field, (c) cut at $y=0$, vy in color and vx, vz indicated by arrows, (d) same as in (c) for the magnetic field, (e) same as in (b) but for a cut at $y=\pi/4$, and (f) same as in (e) for the magnetic field.

These oscillations between the hydrodynamic laminar and turbulent regime in the Roberts flow have been previously found by Feudel *et al.* [8]. The authors pointed out that in this regime, close to the threshold R_M^c the dynamo exhibits an intermittent behavior, with bursts of activity. The oscillatory flow is stable to small perturbations (e.g., numerical noise in the code), but as the magnetic energy grows the flow is perturbed by the Lorentz force and goes to a weakly turbulent regime. As noted in Ref. [8], if R_M is close to R_M^c then the magnetic field decays, the flow relaminarizes and the process is repeated. However, as observed in Fig. 6, if R_M is large enough the weakly turbulent flow can still excite a dynamo, and the magnetic field keeps growing exponentially until reaching the nonlinear saturation even after the hydrodynamic instability takes place.

Figure 8(a) shows the temporal growth of several Fourier components of the magnetic field in the laminar regime ($R_V=63$). A straightforward exponentiation, followed by a flat, steady-state, leveling-off exhibits the same growth rate for all harmonics. This indicates the existence of a simple unstable normal mode which saturates abruptly near $t\approx 180$. The behavior is much noisier for $R_V=420$ and 3300 as shown in Figs. 8(b) and 8(c). Note that in the simulation with $R_V=420$, for $t<70$ all the magnetic modes oscillate with the same frequency as the hydrodynamic oscillations. In Fig. 8, the dotted line and solid line above are, respectively, for $k=1$ and $k=2$. The remaining four are for $k=9$ through 11. The modes in between occupy the open space in between more or less in order. The same modes are shown for $R_V=420$ in Fig. 8(c), which illustrates a broad sharing of E_B among many modes and a consequent excitation of small-scale magnetic components.

Plots of the kinetic and magnetic fields are shown in Fig. 9. The left-hand column shows the velocity field in the saturated state for $R_V=63$, and the right-hand column shows the magnetic field at the same time. The arrows indicate the vector components in the planes shown and the colors indicate the strengths of the perpendicular components. Figures 9(a) and 9(b) are for the plane $z=0$ and Figs. 9(c) and 9(d) are for the plane $y=0$. Figures 9(e) and 9(f) are for the plane $y=\pi/2$. The velocity configuration shown in Fig. 9(a) is quite similar to the way it looks at $t=0$, but the z-dependences apparent in Figs. 9(c), 9(d), and 9(f) are not present in the initial flow.

Figure 10 are similar color plots for the saturated regime for $R_V=420$. All the same quantities are being displayed at the same planes as in Fig. 9. The initial conditions are no longer recognizable in the saturated state, but is not yet sufficiently disordered that one would be forced to call it "turbulent." Moreover, note that the four "cells" characteristic of the laminar Roberts flow [Fig. 9(a)] are not present in this late stage of the dynamo. During the early kinematic regime,

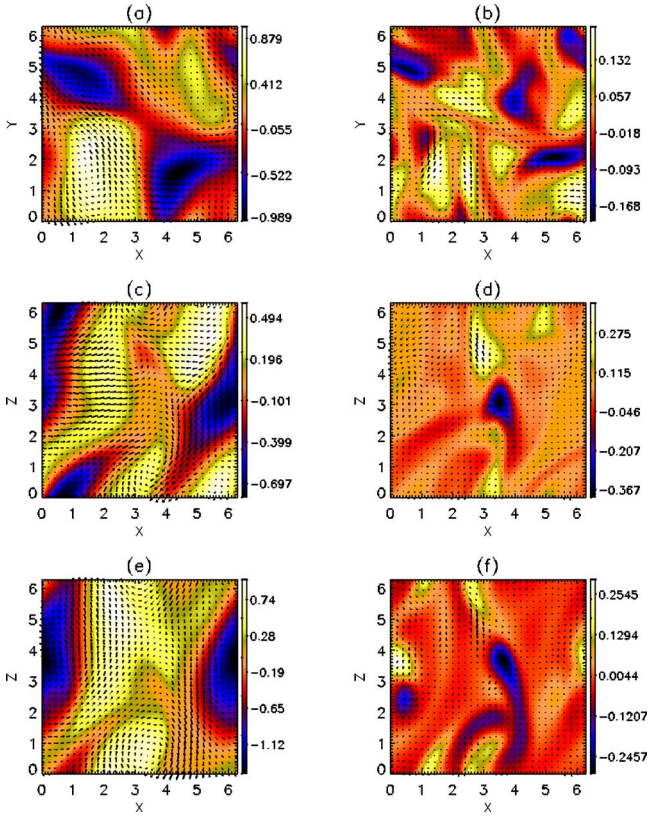

FIG. 10. (Color online) Plots of the kinetic and magnetic fields for the saturated regime of the run with $R_V=R_M=420$. Labels and fields are as in Fig. 9.

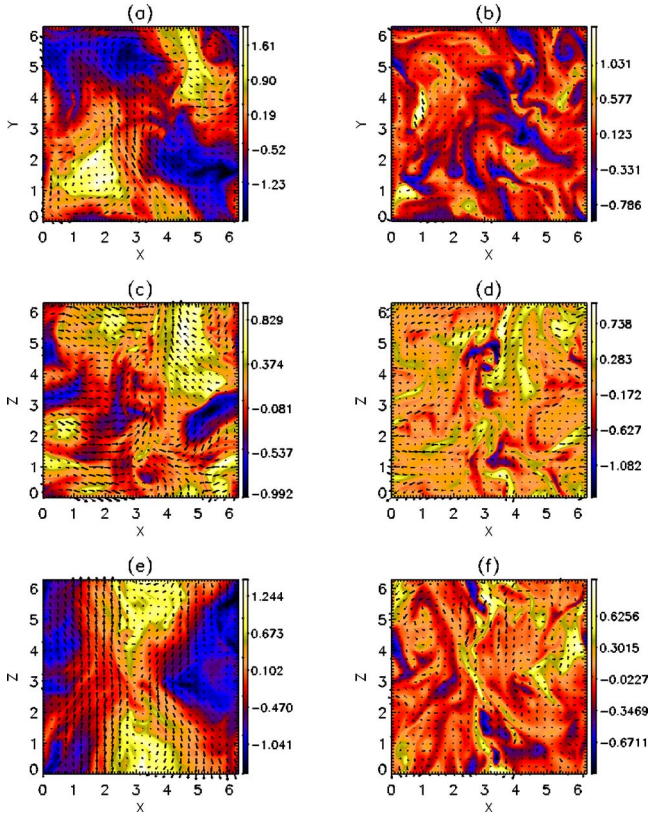

FIG. 11. (Color online) Plots of the kinetic and magnetic fields for the saturated regime of the run with $R_V=3300$ and $R_M=1100$. Labels and fields are as in Fig. 9.

when the hydrodynamic oscillations are observed, a slightly deformed version of these cells can be easily identified in the flow (not shown). When the magnetic energy grows due to dynamo action, the flow is unable to maintain this flow against the perturbation of the Lorentz force. This causes the large-scale flow to destabilize, and the kinetic energy in the shell $k=1$ drops by a factor of 2. This instability of the large-scale modes is associated with the large drop of the kinetic and the total energy at $t\approx 70$ (Fig. 7).

By contrast, the same fields are exhibited in the same planes in Fig. 11 in the saturated regime for $R_V=3300$. Here the truly turbulent nature of the flow is now apparent, particularly in the highly disordered magnetic field plots in the right-hand column.

Figure 12 is a three-dimensional perspective plot of the kinetic and magnetic energy density for $R_V=63$ at a late time in the saturated regime. The kinetic energy distribution (on the left-hand side) is not much different than it was at $t=0$. The helical properties of the Roberts flow can be directly appreciated in the field lines indicated in black. In this regime, the flow is still laminar as previously indicated. The magnetic field is stretched and magnetic energy amplified in the four helical tubes, and then expelled out of the vortex tubes, accumulating in the stagnation points [4,8]. Since the velocity field has no dependence in the z direction, the magnetic field that can be sustained by dynamo action must break this symmetry and displays a clear periodicity in this direction. The same energy densities are exhibited at a late time for the case of $R_V=3300$ in Fig. 13, and the highly filamented and disordered distributions characteristic of the turbulent regime are again apparent. Note however that still some helicity can be identified in the velocity field lines shown.

In Ref. [3] a suppression of small scale turbulent fluctuations and an evolution of the system to a state with effective magnetic Prantdl number of order one was observed in the nonlinear saturation of the turbulent dynamo. Here a similar effect is observed, although the suppression of small scales is weaker probably due to the presence of the external forcing at $k\approx 1$ which does not leave room for a large scale magnetic field to develop. Figure 14 shows the time evolution of the kinetic and magnetic energy spectra in the run with $R_V=3300$ and $R_M=1100$. While at early times the magnetic en-

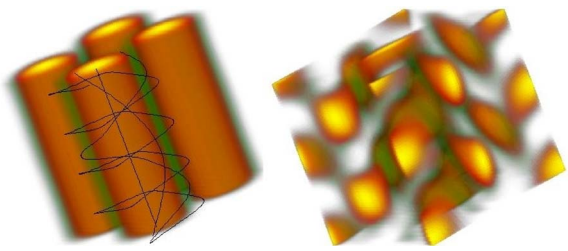

FIG. 12. (Color online) Visualization of the kinetic (left) and magnetic energy density (right) for the saturated regime of the run with $R_V=63$ and $R_M=78$. Velocity field lines are indicated in black.

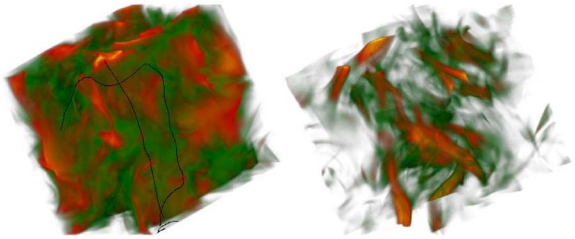

FIG. 13. (Color online) Visualization of the kinetic (left) and magnetic energy density (right) for the saturated regime of the run with $R_V=3300$ and $R_M=1100$. Velocity field lines are indicated in black.

ergy spectrum peaks at small scales ($k\approx 9$), at late times the magnetic spectrum is flat for small k and drops together with the kinetic energy. The kinetic spectrum is strongly quenched and has a large drop at small scales. More details about the interactions between large and small scales are given in the Appendix.

IV. SUMMARY AND DISCUSSION

One apparent outcome of these computations has been to confirm the intuitive impression that dynamo amplification of very small magnetic fields in conducting fluids is easier if mechanical helicity is present (see also Refs. [14–16]). This is true in velocity fields which are both turbulent and laminar. The values of R_M^c which are the lowest found (~ 10) are well below those in several existing experimental searches.

It is also somewhat reassuring to find that the qualitative behavior of dynamo thresholds with decreasing viscosity (increasing Reynolds number at fixed U) is as similar as it is to that found for the nonhelical TG flow in Ref. [1]. In particular, since the simulations discussed here were forced at almost the largest scale available in the periodic domain, a turbulent regime for $P_M<1$ where R_M^c is approximately independent of P_M was reached using only DNS, while for the TG flow two different models [17,18] for the small scales were needed. The similarities in the behavior of the threshold for the two flows for P_M small enough brings more confidence to the ability of subgrid scale models of MHD turbulence to predict results in regimes of interest for astrophysics and geophysics that are today out of reach using DNS. That being said, it should be admitted that the Roberts flow in a way exhibits a richer set of possibilities in that the dynamo activity is somewhat different in each of the three regimes (laminar and steady state, oscillatory, and turbulent).

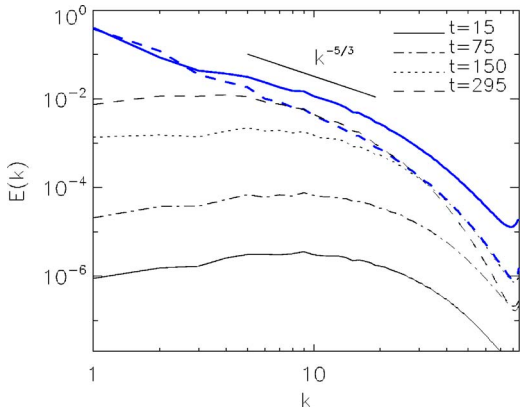

FIG. 14. (Color online) Kinetic [thick (blue) lines] and magnetic energy spectra (thin lines) for different times for the simulation with $R_V=3300$ and $R_M=1100$.

Dynamo action is to be regarded as of many types [3] and situation dependent. The forms of the magnetic fields developed and their characteristic dimensions are determined to a considerable extent by the mechanical activity that excites them and by the geometric setting in which they take place. If it is desired to apply the theoretical and computational results to planetary dynamos or laboratory experiments, then rectangular periodic conditions appear to be a constraint that should be dispensed with as soon as feasible.

ACKNOWLEDGMENTS

The authors are grateful for valuable comments by Dr. Annick Pouquet. The NSF Grant No. ATM-0327533 at Dartmouth College and Grant No. CMG-0327888 at NCAR supported this work in part and are gratefully acknowledged. Computer time was provided by the National Center for Atmospheric Research.

APPENDIX: THE LARGE SCALE FLOW AND THE DYNAMO IN THE TURBULENT REGIME

References [1,3] and the results presented in this paper show that when a large scale flow is present the threshold for dynamo action R_M^c is independent of R_V for values of P_M small enough (compare this result with results using random forcing, e.g., Ref. [19]). One important question that arises is what are the contributions to the dynamo due to the time averaged large scale component of the flow and what are due to the turbulent fluctuations about that average. In experiments using highly constrained flows [6,7] it has become a common practice to use the flow averaged in time to predict the threshold R_M^c, suggesting that perhaps only the large scale flow is responsible for the dynamo amplification. In this Appendix we briefly discuss results for the Roberts flow.

For the simulation in the turbulent hydrodynamic regime with $R_V=1300$, an average in time flow $\bar{\mathbf{v}}$ was computed using 1000 snapshots of the velocity field covering a time span of 600 eddy turnover times in the turbulent steady state. Convergence of $\bar{\mathbf{v}}$ was verified, in the sense that the probability density functions (PDFs) of velocity increments for $\bar{\mathbf{v}}$ were unchanged if the averaging process was continued. Using the averaged flow, kinematic simulations were done solving Eq. (2) where $\mathbf{v}$ was replaced by $\bar{\mathbf{v}}$. Varying the value of the magnetic diffusivity, the threshold for dynamo action using $\bar{\mathbf{v}}$ was determined to be $\bar{R}_M^c=65\pm 1$ (the Reynolds numbers are defined using U and L from the hydrodynamic simulation). This value is close to the threshold for the laminar flow, $R_M^c=62\pm 1$ (see Fig. 1), and far from the threshold measured for the instantaneous flow at $R_V=1300$, where $R_M^c=350\pm 40$, a more than fivefold difference.

The low value of $\bar{R}_M^c$ could suggest that the large scale flow amplifies the magnetic field, while turbulent fluctuations only destroy it and increase the threshold R_M^c. Note however that the average flow $\bar{\mathbf{v}}$ has an infinite correlation time. In the MHD simulations only the external force has an infinite correlation time, while the correlation time of the large scale flow is of order L/U. A detailed analysis of the contribution due to these two components of the flow requires the study of the energy transfer. From Eqs. (1) and (2), we can define the transfer functions (see Ref. [3])

$$T_L(k) = \int \hat{\mathbf{v}}_\mathbf{k} \cdot \widehat{(\mathbf{j} \times \mathbf{B})}_\mathbf{k}^* d\Omega_\mathbf{k}, \tag{A1}$$

$$T_M(k) = \int \hat{\mathbf{B}}_\mathbf{k} \cdot \boldsymbol{\nabla} \times \widehat{(\mathbf{v} \times \mathbf{B})}_\mathbf{k}^* d\Omega_\mathbf{k}, \tag{A2}$$

where the hat denotes Fourier transform, the asterisk complex conjugate, and $d\Omega_\mathbf{k}$ denotes integration over angle in Fourier space. In these definitions, it is assumed that the complex conjugate of the integrals is added to obtain real transfer functions.

Negative values of the function $T_L(k)$ represents energy given by the velocity field at shells with wave number k to the magnetic field at all scales. On the other hand, $T_M(k)$ gives information of both the wave numbers k where magnetic field is being created by stretching, and the nonlinear transfer of magnetic energy to smaller scales. These two contributions to $T_M(k)$ can also be studied separately (see Ref. [20]).

Figure 15 shows the functions $-T_L(k)$ and $T_M(k)$ for the same simulations than Figs. 3 and 4. For the sake of comparison, the transfer functions were normalized using the rms velocity and the mean square magnetic field. In the laminar regime ($R_V \lesssim 100$) $-T_L(k)$ peaks at $k=1$, indicating that kinetic energy is extracted at this shell and given to the magnetic field. $T_M(k)$ peaks at $k=2$, and is nonzero in a narrow band, in good agreement with the magnetic energy spectrum resulting from dynamo action (see Fig. 4). Also in the oscillatory regime ($100 \lesssim R_V \lesssim 1000$) $-T_L(k)$ peaks at $k=1$, but small contributions at $k=2$ and 3 can be identified. Finally, in the turbulent regime ($RV \gtrsim 1000$) $-T_L(k)$ shows a wide range of wave numbers in the velocity field giving energy to the magnetic field. The transfer from the velocity field at $k=1$ to the magnetic field is strongly diminished. Compared with these curves, the average flow gives only energy to the magnetic field from the shell with $k=1$ (not shown). In the turbulent regime, also the peak in $T_M(k)$ moves to larger wave numbers and covers a wider range of scales. A more detailed analysis of the interactions between length scales requires the study of shell-to-shell energy transfers, and is presented elsewhere [20,21].

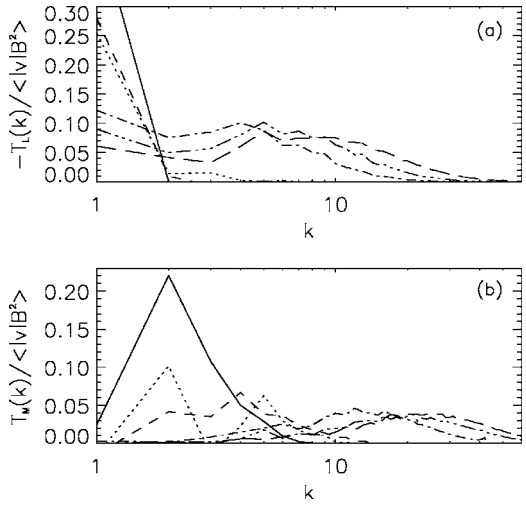

FIG. 15. Normalized transfer functions (a) $-T_L(k)$, and (b) $T_M(k)$ for different runs in the kinematic regime. Labels of the curves are as in Figs. 3 and 4.

[1] Y. Ponty, P. D. Mininni, D. C. Montgomery, J.-F. Pinton, H. Politano, and A. Pouquet, Phys. Rev. Lett. **94**, 164502 (2005).
[2] G. I. Taylor and A. E. Green, Proc. R. Soc. London, Ser. A **158**, 499 (1937).
[3] P. D. Mininni, Y. Ponty, D. C. Montgomery, J. F. Pinton, H. Politano, and A. Pouquet, Astrophys. J. **626**, 853 (2005).
[4] G. O. Roberts, Philos. Trans. R. Soc. London, Ser. A **271**, 411 (1972).
[5] M. L. Dudley and R. W. James, Proc. R. Soc. London, Ser. A **425**, 407 (1989).
[6] A. Gailitis, O. Lielausis, E. Platacis, S. Dement'ev, A. Cifersons, G. Gerbeth, T. Gundrum, F. Stefani, M. Christen, and G. Will, Phys. Rev. Lett. **86**, 3024 (2001).
[7] R. Stieglitz and U. Muller, Phys. Fluids **13**, 561 (2001).
[8] F. Feudel, M. Gellert, S. Rudiger, A. Witt, and N. Seehafer, Phys. Rev. E **68**, 046302 (2003).
[9] S. A. Orszag, Stud. Appl. Math. **51**, 253 (1972).
[10] S. A. Orszag and J. G. S. Patterson, Phys. Rev. Lett. **28**, 76 (1972).
[11] C. Canuto, M. Y. Hussaini, A. Quarteroni, and T. A. Zang, *Spectral Methods in Fluid Dynamics* (Springer-Verlag, New York, 1988).
[12] D. O. Gómez, P. D. Mininni, and P. Dmitruk, Phys. Scr., T **T116**, 123 (2005).
[13] B. Galanti, P.-L. Sulem, and A. Pouquet, Geophys. Astrophys. Fluid Dyn. **66**, 183 (1992).
[14] H. K. Moffatt, *Magnetic Field Generation in Electrically Conducting Fluids* (Cambridge University Press, Cambridge, 1978).
[15] A. Brandenburg, Astrophys. J. **550**, 824 (2001).
[16] V. Archontis, S. B. F. Dorch, and A. Nordlund, Astron. Astrophys. **410**, 759 (2003).
[17] P. D. Mininni, D. C. Montgomery, and A. Pouquet, Phys. Rev. E **71**, 046304 (2005).

[18] Y. Ponty, H. Politano, and J.-F. Pinton, Phys. Rev. Lett. **92**, 144503 (2004).

[19] A. Schekochihin, N. Haugen, A. Brandenburg, S. Cowley, J. Maron, and J. McWilliams, Astrophys. J. **625**, L115 (2005).

[20] A. Alexakis, P. D. Mininni, and A. Pouquet, Phys. Rev. E **72**, 046301 (2005).

[21] P. D. Mininni, A. Alexakis, and A. Pouquet, Phys. Rev. E **72**, 046302 (2005).